




Dependence of evanescent wave polarization on the losses of guided optical modes

Sinuhé Perea-Puente  and Francisco J. Rodríguez-Fortuño ^{*}

Department of Physics, King's College London, Strand, London WC2R 2LS, United Kingdom

 (Received 24 February 2021; revised 12 July 2021; accepted 14 July 2021; published 13 August 2021)

Spin-momentum locking of evanescent waves describes the relationship between the propagation constant of an evanescent mode and the polarization of its electromagnetic field, giving rise to applications in light nanorouting and polarimetry among many others. The use of complex numbers in physics is a powerful representation in areas, such as quantum mechanics or electromagnetism; it is well known that a lossy waveguide can be modeled with the addition of an imaginary part to the propagation constant. Here we explore how these losses are entangled with the polarization of the associated evanescent tails for the waveguide, revealing a well-defined mapping between waveguide losses and the Poincaré sphere of polarizations in what could be understood as a “polarization-loss locking” of evanescent waves. We analyze the implications for near-field directional coupling of sources to waveguides as optimized dipoles must take into account the losses for a perfectly unidirectional excitation. We also reveal the potential advantage of calculating the angular spectrum of a source defined in a complex rather than the traditionally purely real transverse wave-vector space formalism.

DOI: [10.1103/PhysRevB.104.085417](https://doi.org/10.1103/PhysRevB.104.085417)

I. INTRODUCTION

Since the birth of nanoscience in the latter decades of the twentieth century, it is possible to revisit some old well-established theoretical concepts and exploit them for novel near-field applications in subwavelength phenomena. In particular, consider the case of evanescent waves [1], known more than 150 yr ago and traditionally considered as a mere theoretical corollary in total internal reflection situations. In recent years, evanescent waves have become deeply reenvisioned as fascinating and promising tools for optical applications on the nanoscale. Apart from carrying linear and angular momenta in the direction of propagation, evanescent waves were lately shown to also transport a transverse spin angular momentum [2–5], leading to spin-momentum locking [6,7] (also known as the photonic quantum spin Hall effect [6] in line with its electronic counterpart).

Spin-momentum locking is one of the most promising features of evanescent waves as it is an inherent property independent of their source. It has been experimentally demonstrated that spin-momentum locking occurs in a wide range of physical systems, such as surface-plasmon polaritons [8], optical fibers [7,9,10], and silicon waveguides [11]. It plays a key role enabling selective coupling in the near and far fields via polarized dipoles [8,12], giving rise to recoil optical forces [13–16] and presents further applications in other areas, such as optical isolation [17,18], nanopolarimetry [19], or optical vortex emitters [20]. We also note that the underlying physics applies to wave fields beyond electromagnetism, such as acoustics [21,22] and gravitational waves [23].

The spin-momentum locking of evanescent tails in a waveguided mode ultimately stems from the transversal-

ity condition of momentum eigenmodes, $\mathbf{k} \cdot \mathbf{E} = \mathbf{k} \cdot \mathbf{H} = 0$, relating the wave-vector \mathbf{k} to the electric-field \mathbf{E} and magnetic-field \mathbf{H} polarization of the mode [6]. Therefore, the propagation constant of the waveguide mode k_m is crucial because momentum conservation in translationally invariant waveguides requires that the component of the evanescent field's wave vector in the propagation direction k_x must be equal to the intrinsic propagation constant of the mode as depicted in Fig. 1. In recent literature [3,7], lossless waveguide modes are typically considered—which means that the propagation constant k_m , and, hence, k_x too, is taken as a real number. In this well-known situation, the total wave vector of the evanescent wave still exhibits complex-number behavior due to the wave-vector \mathbf{k} having an imaginary component in the perpendicular direction to the guided mode k_z , corresponding to the direction of evanescent attenuation, whereas having a purely real component in the propagation direction k_x . As we know, both components are related via the wave-equation $\mathbf{k} \cdot \mathbf{k} = k^2$, where $k = n\omega/c$ is the background wave number for a medium with refractive index n . However, more degrees of freedom can be gained if one considers complex propagation constants corresponding to lossy waveguides. Mathematically, a lossy waveguide is simply associated with a complex propagation constant. This, in turn, implies a complex wave-vector component in the propagation direction $k_x = k'_x + ik''_x$ for the evanescent wave. In this case, to satisfy the wave equation, both k_x and k_z wave-vector components acquire both real and imaginary parts, which, therefore, affects the polarization properties and the spin of the associated evanescent waves via the transversality conditions. Although this is an expected result, or, at least, should not be surprising, in this paper we wish to study the phenomenon in depth to uncover its subtleties. In particular, we will see that the presence of losses must be taken into account when designing a dipole for optimal directionality in evanescent coupling.

^{*}Corresponding author: francisco.rodriguez-fortuno@kcl.ac.uk

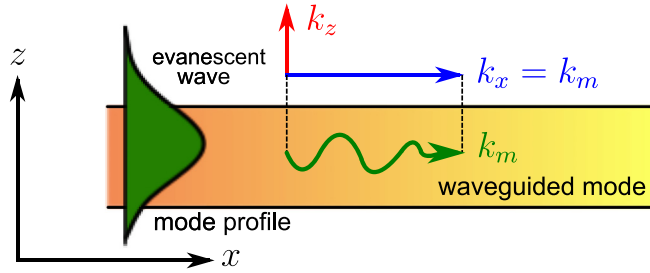


FIG. 1. Evanescent tail of a two-dimensional- (2D-) slab waveguide showing the relation between the evanescent wave-vector $\mathbf{k} = k_x \hat{\mathbf{x}} + k_z \hat{\mathbf{z}}$ and the waveguide propagation constant k_m .

This paper is split into two main parts. First, we will analyze the polarization in the evanescent tail for a lossy waveguide. We will study the geometric paths described in the Poincaré sphere by this polarization as the losses of the waveguide are varied. Second, we will study evanescent coupling between a dipole source and a lossy waveguide, exploring the effects of loss in the guided mode, and how the dipole optimization and tunability for selective control of unidirectional excitation should be recalculated in this scenario. For this, we will use both Fermi's golden rule [24,25] and the angular spectrum approach [8,12,15,21,26], which we will here extend to a complex domain. We will prove that the dipole polarization must be reoptimized taking into account the losses for a perfect contrast directionality and this optimization can be associated with a zero in a complex domain of the angular spectrum.

II. POLARIZATION PATHS FOR THE EVANESCENT TAILS OF A LOSSY WAVEGUIDE

In our first approach, we will calculate the polarization ellipse for the evanescent tails of a lossy waveguide. In order to get at the essence of the phenomenon, we will study the simplest possible scenario, a two-dimensional problem as shown in Fig. 1 where a slab waveguide is embedded in an infinite-homogeneous background of refractive index n . In our calculations we take $n = 1$ for simplicity, i.e., free space surroundings. The lossy waveguide supports a well defined time-harmonic mode defined by its propagation constant $k_m = k'_m + ik''_m$. The propagator in the waveguide is given by $e^{i(k_mx - \omega t)} = e^{ik'_m x} e^{-i\omega t} e^{-k''_m x}$, clearly exhibiting phase propagation in space associated to the propagation constant k'_m , time-harmonic phase advance in time due to the real-valued angular frequency ω , and an evanescent amplitude decay in space corresponding to the attenuation constant k''_m caused by waveguide mode losses. The evanescent tails of such a mode can be written as a momentum eigenvector in complex phasor notation as $\{\mathbf{E}_{\text{ev}}(\mathbf{r}), \mathbf{H}_{\text{ev}}(\mathbf{r})\} = \{\mathbf{E}_0, \mathbf{H}_0\} e^{i\mathbf{k} \cdot \mathbf{r}}$, where \mathbf{E}_0 and \mathbf{H}_0 are the evanescent wave electric and magnetic-field polarization, \mathbf{k} is the wave vector of the evanescent wave, and \mathbf{r} is the position vector. Such a momentum eigenvector must be a solution to Maxwell's equations, and as such it must fulfill two important requirements:

$$\mathbf{k} \cdot \mathbf{k} = k^2 \quad \text{and} \quad \mathbf{k} \cdot \mathbf{E}_{\text{ev}} = \mathbf{k} \cdot \mathbf{H}_{\text{ev}} = 0. \quad (1)$$

The first requirement comes from the homogeneous Helmholtz wave equation derived [27] from Maxwell's

equations, and the second comes from Gauss' law in the absence of sources, also known as the transversality condition [7]. Note, as is well known, that the first equation acts on a complex wave vector, so it is not the analytical equation of a circumference.

To simplify the situation further we will consider only a transverse-magnetic [(TM) or p] mode, in which the magnetic-field polarization of the evanescent wave is trivial $\mathbf{H}_0 = H_y \hat{\mathbf{y}}$ and the electric field is responsible for all the interesting polarization phenomena and transverse spin $\mathbf{E}_0 = E_x \hat{\mathbf{x}} + E_z \hat{\mathbf{z}}$. This apparent loss of generality is justified because a transverse-electric [(TE) or s] mode would show identical phenomena, but simply switching the roles between \mathbf{E}_0 and \mathbf{H}_0 . Hence, in our simplified case of a TM mode and 2D problem $\mathbf{k} = k_x \hat{\mathbf{x}} + k_z \hat{\mathbf{z}}$, the above conditions in Eq. (1) can be simplified to

$$k_x^2 + k_z^2 = k^2 \quad \text{and} \quad k_x E_x + k_z E_z = 0. \quad (2)$$

With these equations, together with the fact that $k_x = k_m$ due to conservation of momentum parallel to the axes of translational invariance in the waveguide, we are able to study all the changes in the polarization of the evanescent tails with the addition of losses to the waveguide. In order to illustrate this behavior, we map a grid in the complex plane of propagation constants [Fig. 2(a), corresponding to any possible propagating mode] to the associated transverse polarization that the evanescent tail would have for that mode, in the Poincaré sphere as shown in Fig. 2(b) (see Appendix A for detailed calculations). The plane of polarization ellipses used to calculate the Stokes parameters to depict the Poincaré sphere is taken as the (x, z) plane, parallel to the propagation direction x as expected for the electric field of a p -polarized evanescent mode.

To analyze Fig. 2, we highlight as a blue line the well-known case of lossless waveguided modes, corresponding to a real $k_m/k \in [1, \infty)$. When $k_m/k = 1$, this is not a guided mode but a propagating plane wave with linear p polarization, hence, we are in the equator of the Poincaré sphere. When $k_m/k > 1$ is increased, making the wave more and more evanescent (i.e., decaying more strongly), the polarization of the evanescent wave follows a geodesic path, moving towards the upper pole, where $S_3/S_0 = 1$ corresponding to purely circular polarization in the Poincaré sphere, in agreement with the well-known appearance of a transverse spin. When losses are added, it is interesting that the polarization moves away from the $S_2 = 0$ condition [7] as k_z is not purely imaginary characteristic of lossless modes. The presence of nonzero S_2 indicates a tilting of the polarization ellipse due to the losses. As losses are increased, the polarization follows a cardioidlike path in the Poincaré sphere also tending to the upper pole in the limit of high losses.

To illustrate this effect, in Figs. 2(a) and 2(b) we select four distinct locations $\{A, B, C, D\}$, corresponding to modes with $k_m/k = 1.2 + \{0, 0.5, 1, 1.5\}i$, varying the amount of losses. The polarization ellipse for the electric field of the evanescent tail of such a mode is plotted in Fig. 2(c), noting that the local polarization of the electric field tilts and depends strongly on the losses of the waveguide.

These results are very general because the electromagnetic equations governing the evanescent tails of planar waveguides

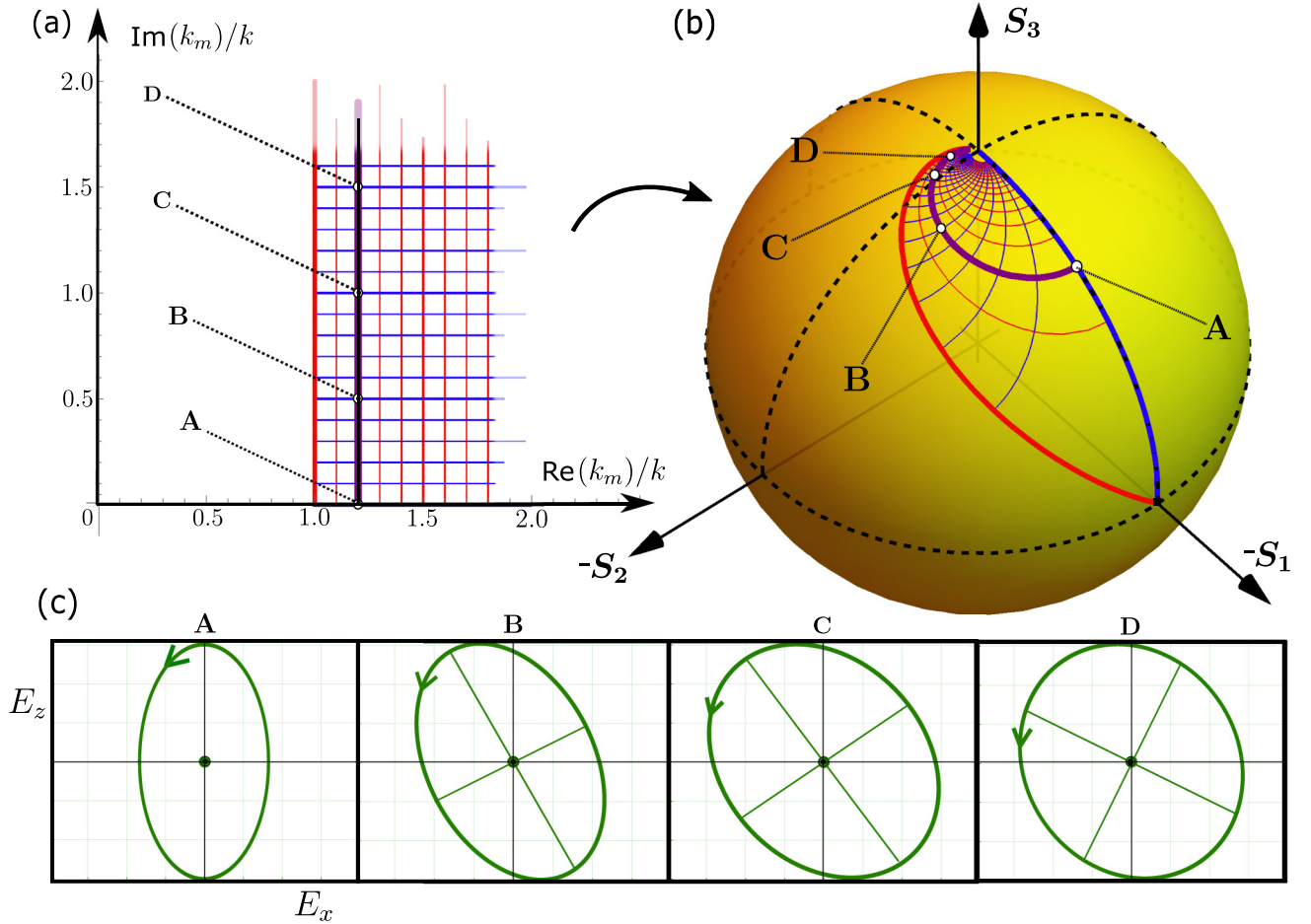


FIG. 2. Evanescent wave polarization in the Poincaré sphere from normalized Stokes parameters $\{S_1, S_2, S_3\}/S_0$ (b) as the propagation constant of the waveguide mode is varied in the complex plane (a) where the red and blue lines represent a mesh on the complex k_m plane, mapped into the Poincaré sphere. The thick blue line represents the line $k_m \in [1, \infty)$ whereas the red and purple thick lines represent varying imaginary parts for $k'_m/k = 1$ and $k'_m/k = 1.2$, respectively. A selection of four points $\{A, B, C, D\}$ have been chosen as an example with propagation constants $k_m/k = 1.2 + \{0-3\} \frac{i}{2}$ showing the influence of the imaginary part of k_m (waveguide losses k''_m) on the polarization. The corresponding electric-field polarization ellipse is shown in (c).

depend only on the propagation constant k_m and not on the specific nature of the waveguide. The results are, therefore, waveguide independent, and although we illustrated a slab waveguide in Fig. 1, the analytical equations and results, including the mapping shown in Fig. 2, are valid for any planar waveguide setup including slab waveguides and plasmonic films.

The above analysis of the polarization of evanescent tails was performed for the simple case of planar waveguides to keep the discussion clear and easy to grasp, but analogous considerations hold, in general, for other waveguide geometries. For instance, considering cylindrical waveguides, such as optical fibers or plasmonic nanowires where the mode propagates along the z direction, we can briefly outline a methodology to arrive at similar results. The general solution to the scalar wave equation in cylindrical coordinates is given by [28]

$$\Psi(\rho, \varphi, z) = [A_1 J_\ell(k_\rho \rho) + A_2 Y_\ell(k_\rho \rho)] \times (B_1 e^{i\ell\varphi} + B_2 e^{-i\ell\varphi}) e^{ik_z z}, \quad (3)$$

where J_ℓ and Y_ℓ correspond to the Bessel functions of the first and second kinds, and analogously to Eq. (2) there is also a relation between k_ρ and k_z given by

$$k_\rho^2 + k_z^2 = k^2. \quad (4)$$

The propagation constant of the mode, being $k_z = k_m$, will be complex in a lossy mode, which will affect the value of k_ρ and this, in turn, will affect the polarization of the mode. This requires solving the vector components for the vectorial wave equation. For instance, in TM_z modes, the solution $\Psi(\rho, \varphi, z)$ described above can refer to the vector potential $\mathbf{A} = \Psi \hat{\mathbf{z}}$ and the different electric-field polarization components will depend directly on various spatial derivatives of Ψ with respect to ρ , φ , and z [28], which, of course, will be directly affected by k_ρ and k_z being complex. Hence, the local mode polarization of the evanescent tails will be affected by the mode losses in cylindrical waveguides too. This trend indicates that this is a general phenomenon for any type of waveguide.

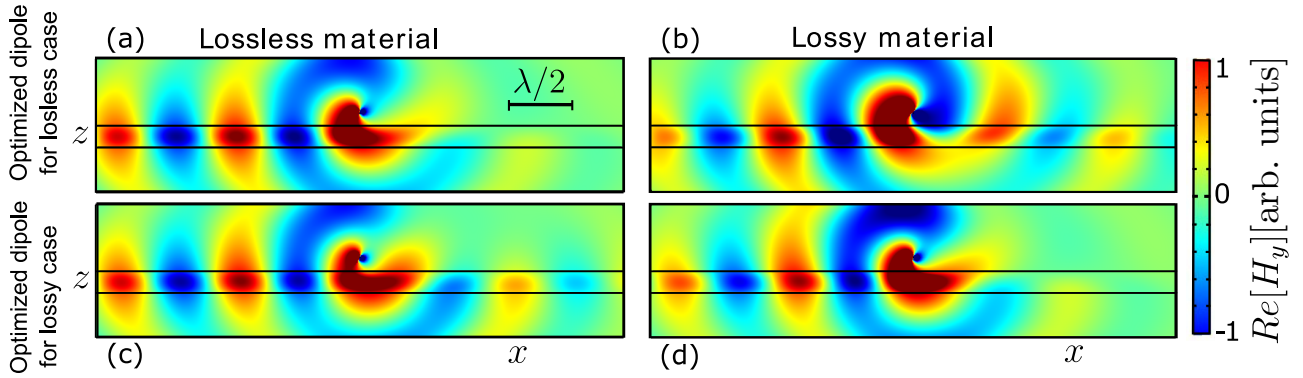


FIG. 3. Dielectric slab waveguide with thickness $t = \lambda/6$ placed on free space, excited by a dipole source $d = \lambda/10$ from the dielectric with a varying dipole optimization (up/bottom) and amount of dielectric losses (left/right). In the left column, a lossless material is considered with refractive index $n_1 = 2$, whereas in the right column a lossy material with $n_2 = 2 + 0.3i$ is used. The dipoles were optimized via Fermi's golden rule for near-field selective vectorial coupling to the left side. The upper row has a dipole $\mathbf{p}_1 \approx (1.11, 0, 0.49i) \propto \mathbf{k}_{\text{lossless}}^*$ whereas the lower row has $\mathbf{p}_2 \approx (1.10, 0, 0.11 + 0.47i) \propto \mathbf{k}_{\text{lossy}}^*$. Clear unidirectionality is shown in (a) and (d) with theoretically contrast ratio 1:0 whereas in (b) and (c) an “undesired” back-excitation is observed with an expected contrast of 1:0.14. The color scale (arbitrary units) is the same for all plots. For the simulation, the COMSOL WAVE OPTICS module was used.

III. NEAR-FIELD COUPLING DIPOLE OPTIMIZATION

Now, the fact that the polarization of the evanescent electric field in the waveguide depends on losses has evident implications for unidirectional coupling of dipoles near the surface. Consider a pointlike dipole with polarization given by $\mathbf{p} = (p_x, p_y, p_z)$ placed in the evanescent region of the slab waveguide at a height d above the dielectric slab waveguide of thickness t . As is known [8], suitably optimized elliptical dipoles can be used to achieve the unidirectional excitation of the guided modes. Here we ask how this phenomenon is affected by the losses in the waveguide.

Figure 3 shows a numerical simulation of the effect of losses on dipolar directional excitation. Note that our modeling assumes a point dipole model with a given polarization vector as the source of fields for theoretical simplicity. Experimentally, a point dipole source with desired polarization can be recreated from the scattering of illuminated small metallic or dielectric scatterers in the Rayleigh regime, using suitably designed polarized illumination [10,29,30]. Figure 3(a) corresponds to the known case of a lossless waveguide being excited by an optimized elliptical dipole, exhibiting perfect directionality. Figure 3(b) shows exactly the same dipole but with losses added to the waveguide. One can see that due to the presence of losses the dipole is no longer perfectly unidirectional, i.e., it does not exhibit a 100% contrast ratio between left and right excitations. This is because the polarization of the evanescent tails of the waveguides have changed, and, hence, the optimization of the dipole must take this into account. In Fig. 3(d), the dipole polarization has been adjusted to account for the losses, and this time one sees, indeed, a perfect directionality. This dipole, whose polarization is adjusted for losses, will not work in the lossless waveguide as shown in Fig. 3(c). The results convincingly show that dipole directionality must necessarily take losses into account if one wants to achieve perfect directionality. Next we explain how to deduce this, following two complementary methods: Fermi's golden rule and the dipole angular spectrum.

In the context of dipolar coupling to waveguides, Fermi's golden rule approaches states [24,25] that the excitation amplitude of a mode with electric-field $\mathbf{E}(\mathbf{r})$ by a dipole \mathbf{p} located at \mathbf{r}_0 is proportional to $\mathbf{p}^* \cdot \mathbf{E}(\mathbf{r}_0)$ such that the intensity is proportional to $|\mathbf{p}^* \cdot \mathbf{E}(\mathbf{r}_0)|^2$. Following this approach, one can achieve perfect contrast directionality of excitation simply by choosing a dipole polarization that cannot couple to the evanescent wave propagating along one direction in the waveguide. This is achieved when $\mathbf{p} \propto \mathbf{k}^*$; with this condition, following Gauss' law requirement from Eq. (1), we can see that $\mathbf{p}^* \cdot \mathbf{E}_{\text{ev}} \propto \mathbf{k} \cdot \mathbf{E}_{\text{ev}} = 0$. In our simplified 2D case, this means $\mathbf{p} \propto (k_x^*, 0, k_z^*) = (\pm k_m, 0, \sqrt{k^2 - k_m^2})^*$ with the plus or minus sign determining which of the two directions of mode propagation, right or left, we wish the dipole to not couple to. The polarization of the optimized dipole, therefore, depends directly on the losses of the waveguide via k_m and this is the optimized dipole used in the numerical simulations of Figs. 3(a) and 3(d).

The above argument using Fermi's golden rule fully explains why taking losses into account is important for dipole directionality, but next we will also analyze the same phenomenon from the dipole angular spectrum approach. This is often used as an alternative explanation to directionality—giving the same results, but offering a different perspective, as it reveals that directionality can be a property of the dipole itself, independent of the waveguide mode [2,8]. The directionality of the dipole can be then associated with a zero amplitude at a specific location in the angular spectrum of the dipole source. This specific location is determined by the waveguide mode. This approach offers an intuitive way to design the directionality of multimode waveguides [31] by setting sources with zero amplitudes at the angular spectrum location corresponding to the propagation constant of each mode. However, this approach comes with a problem when considering lossy modes because the propagation constant of the mode is a complex number, whereas the angular spectrum of a source $\mathbf{E}^{\text{dipole}}(k_x, k_y)$ is defined on the real plane of

transverse wave-vectors (k_x, k_y) as follows [32]:

$$\mathbf{E}^{\text{dipole}}(\mathbf{r}) = \iint_{-\infty}^{\infty} \mathbf{E}^{\text{dipole}}(k_x, k_y) e^{i(k_x x + k_y y + k_z z)} dk_x dk_y, \quad (5)$$

where $\mathbf{E}^{\text{dipole}}(\mathbf{r})$ are the spatial fields of a dipole in free space and $k_z = \pm\sqrt{k^2 - k_t^2}$ with $k_t^2 = k_x^2 + k_y^2$ being the transverse wave vector and choosing the sign of k_z depending on the one of z .

The question we ask is, can we study the angular spectrum of the dipole beyond real values of k_x and k_y to study its coupling to lossy modes? Can we define and calculate an angular spectrum defined for complex values in the transverse momentum plane? The definition of the angular spectrum in Eq. (5) requires an integral on the real plane (k_x, k_y) , however, nothing is stopping us from taking the known analytical form of the angular spectrum of a dipole, which is defined in terms of k_x and k_y and calculating it for complex values of k_x . The angular spectrum of an electric dipole source with dipole moment \mathbf{p} is well known (see a concise derivation on Appendix B),

$$\mathbf{E}^{\text{dipole}}(k_x, k_y) = \frac{i}{8\pi^2 \varepsilon} \frac{k^2}{k_z^{(+)}} [(\mathbf{p} \cdot \hat{\mathbf{e}}_p) \hat{\mathbf{e}}_p + (\mathbf{p} \cdot \hat{\mathbf{e}}_s) \hat{\mathbf{e}}_s], \quad (6)$$

where $k_z^{(+)}$ indicates taking the sign of k_z that corresponds to positive z , ε is the electric permittivity of the medium and the two unit vectors $\hat{\mathbf{e}}_p = (\frac{k_x k_z}{k k_t}, \frac{k_y k_z}{k k_t}, -\frac{k_z}{k})$ and $\hat{\mathbf{e}}_s = (-k_y/k_t, k_x/k_t, 0)$ represent the p -polarized and s -polarized unit vectors [12,33], remembering to choose the sign of k_z according to whether we are calculating the field in the upper hemisphere with $z > 0$ or the lower one, where $z < 0$.

If one designs a dipole \mathbf{p} optimized for generating a perfect directionality inside a lossless waveguide mode with a certain real value of propagation constant k_m , such as the dipole in Fig. 3(a), then the dipole angular spectrum shows a zero amplitude at $(k_x, k_y) = (k_m, 0)$ as shown in Fig. 4(a). This was known since the early designs of directional dipoles [8] but in that same work, the presence of losses was identified as a challenge for unidirectionality. The broadening of the waveguide mode's spatial Fourier spectrum in the real k_x axis due to the losses suggested that one cannot design a dipole source to achieve perfect directionality in a lossy waveguide. After all, where should we place this zero in order to cover the entire broadened range of wave vectors spanned by the lossy mode? The answer is that we need to reinterpret the broadening of the mode as a shift of its position away from the real axis and going into the complex domain of k_x . Then it is still possible to design a dipole whose angular spectrum has a zero on the exact location of the mode within the complex domain, enabling the design of perfect directionality even for lossy waveguides as shown in Fig. 4(b). The dipole designed using this method matches exactly with the one designed using Fermi's golden rule previously. In this figure, the angular spectrum is plotted, using Eq. (6) for a dipole that is designed as described above to show optimized directionality on a lossy waveguide. Instead of calculating the spectrum on the real (k_x, k_y) plane as is conventional for angular spectra, we have also calculated the spectrum on the Argand plane of k_x . Interestingly, although the angular spectrum does not show any zero amplitude in the real plane of (k_x, k_y) , it does

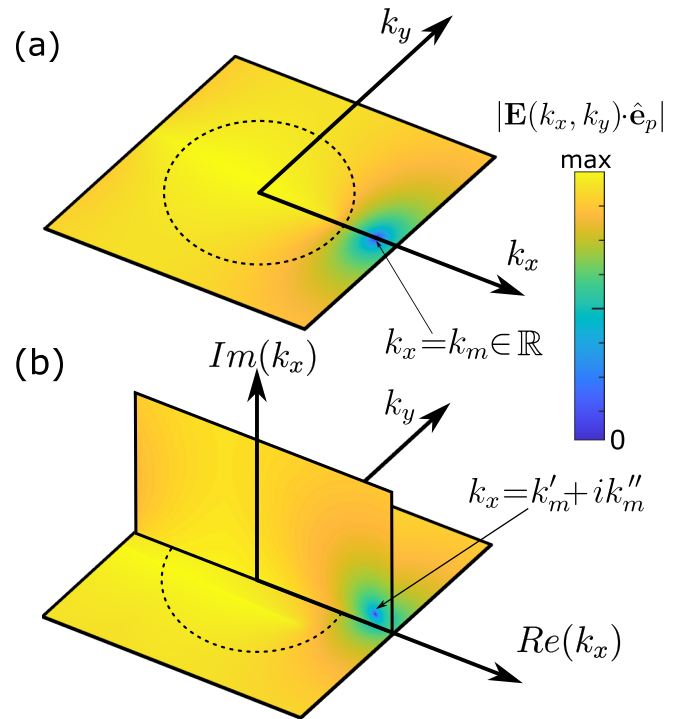


FIG. 4. Angular spectrum $|\mathbf{E}(k_x, k_y) \cdot \hat{\mathbf{e}}_p|$ for a dipole optimized to show perfect contrast directionality for a p -polarized mode that is (a) lossless with $k_m \in \mathbb{R}$ and (b) lossy with $k_m = k'_m + ik''_m$ (so $k_m \in \mathbb{C}$). In (b) the angular spectrum does not show zero amplitude at any location on the (k_x, k_y) real plane (the traditional domain of the angular spectrum), but it does show a zero amplitude if we calculate the spectrum on the complex k_x plane.

show a zero amplitude at the complex point $k_x = k'_m + ik''_m$, as clearly seen in the figure. This indicates that, although the procedure to calculate the fields from the angular spectrum [Eq. (5)] involves using only the real values of k_x and k_y , the information contained in the angular spectrum $\mathbf{E}(k_x, k_y)$ is still meaningful when one considers complex values for the arguments k_x and k_y , at least, in terms of predicting the source's unidirectionality.

IV. DISCUSSION

Using an analogy with the phenomenon of spin-momentum locking in which the spin and polarization of the evanescent wave depends on the propagation direction, we see that the spin and polarization also depend on the losses of the waveguide, showing a phenomenon that we could call polarization-loss locking. It is very interesting to note that the losses of a waveguide can be analytically derived from simply looking at the polarization of the mode at a single fixed point (and vice versa). This allows one to deduce the amplitude decay or spatial gradients of a mode simply with a local precise measurement of polarization, not even requiring the measurement of polarization over a small neighborhood. The local polarization at every point is uniquely mapped with a one-to-one correspondence to the complex propagation constant.

We also showed how this polarization-loss relation must be taken into account when designing near-field dipole directionality and carefully described how this is consistent with existing frameworks of dipole directionality. In particular, it required us to stretch the definition of angular spectra, intriguingly showing some evidence that the calculation of angular spectra in complex variables might have physical significance.

We note that the mode polarization is especially sensitive when the propagation constant is near the threshold with propagating waves $k_m = k_m^0 \gtrsim 1$, corresponding to weakly confined modes. In that case, tiny changes in either the real part ($k_m = k_m^0 + \epsilon$) or the imaginary part ($k_m = k_m^0 + i\epsilon$) (with $0 < \epsilon \in \mathbb{R}$) of the propagation constant will result in comparably large changes in the corresponding polarization of the evanescent wave, which can be translated into significant variations in dipolar coupling to waveguided modes. This suggests that a modulation of intensity could be achieved using directional dipole sources near a waveguide whose real or imaginary part of the refractive index are changed via a material nonlinearity as well as a potential way to encode information on spatial variations of optical losses of a material, whose readout can be realized optically via directional sources.

It is always interesting to see physical phenomena arise when extending variables that are typically considered real into the complex domain. Further research is envisaged exploiting the unidirectional coupling not only in lossy waveguides as performed here, but also lossy surrounding media as well when the waveguide is embedded in a complex refractive index or other possibilities, such as near-zero index materials [34]. In this case, the wave-equation condition $\mathbf{k} \cdot \mathbf{k} = k^2$ becomes even more interesting because the right-hand-side wave number may become complex itself, so \mathbf{k} acquires more degrees of freedom, and new exotic nanophotonic phenomena could arise.

ACKNOWLEDGMENTS

S.P.-P. wants to thank I. Cajiao-Valle for the computer-assisted graphic design tutorials, J. J. Kingsley-Smith for his advice on computational plot representation and a fruitful discussion, D. Martínez-Rubio for a mathematical discussion in the Poincaré sphere, Dr. M. F. Picardi for the suggestions on the dielectric unidirectional model, and Dr. L. Wei for the useful advice given in the numerical simulation of the materials. This work was supported by European Research Council Starting Grant No. ERC-2016-STG-714151-PSINFONI and EPSRC-UK. The authors declare no competing financial interest.

APPENDIX A: STOKES PARAMETER DEPENDENCE ON THE PROPAGATION CONSTANT

In order to calculate the Stokes parameters of the evanescent tail electric field employed to plot the paths on the Poincaré sphere in Fig. 2, we used the definition of Stokes parameters [35,36] but applied on the (x, z) plane where the

electric field lies,

$$\begin{pmatrix} S_0 \\ S_1 \\ S_2 \\ S_3 \end{pmatrix} = \begin{pmatrix} E_x E_x^* + E_z E_z^* \\ E_x E_x^* - E_z E_z^* \\ E_x E_z^* + E_z E_x^* \\ iE_x E_z^* - iE_z E_x^* \end{pmatrix}. \quad (\text{A1})$$

According to the conditions in Eq. (2), it is easy to see that, once k_m is fixed, and, hence, $k_x = k_m$, then we can calculate $k_z = \sqrt{k^2 - k_x^2}$ using the Helmholtz condition [such that $\text{Im}(k_z) \geq 0$] and then the electric field is restricted by the transversality condition to $\mathbf{E}_0 = A_0(\hat{\mathbf{y}} \times \mathbf{k}) = A_0(-k_z, 0, k_x)$ where A_0 is an arbitrary scaling factor. Substituting this into the Stokes parameters in Eq. (A1) results in parametric paths of polarization along the Poincaré sphere as a function of mode propagation constant $\mathbf{S}(k_m) = (S_0, S_1, S_2, S_3)$ used to generate the paths in Fig. 2,

$$\begin{pmatrix} S_0 \\ S_1 \\ S_2 \\ S_3 \end{pmatrix} = \begin{pmatrix} |k_z|^2 + |k_x|^2 \\ |k_z|^2 - |k_x|^2 \\ -2 \text{Re}(k_x^* k_z) \\ 2 \text{Im}(k_x^* k_z) \end{pmatrix} = |k_m|^2 \begin{pmatrix} |\eta|^2 + 1 \\ |\eta|^2 - 1 \\ -2 \text{Re}(\eta) \\ 2 \text{Im}(\eta) \end{pmatrix}, \quad (\text{A2})$$

where superscript $*$ means complex conjugation, $|\cdot|$ means the complex Euclidean modulus, and we have used the ratio [37],

$$\eta(k_m) = \frac{k_z}{k_x} = \frac{\sqrt{k^2 - (k'_m + ik''_m)^2}}{k'_m + ik''_m}, \quad (\text{A3})$$

with special care taken to always take the square root sign that guarantees a positive imaginary part of k_z to ensure a physically meaningful evanescent wave above the waveguide (the opposite sign should be used for the evanescent wave below the waveguide). From here, many analytical limits in the Poincaré sphere can be mathematically obtained. In the propagating plane-wave case $k_m/k = 1$, η becomes null, so $S_2/S_0 = S_3/S_0 = 0$ and analogously $S_1/S_0 = -1$. In the limit of growing lossless mode propagation constant $k'_m \rightarrow \infty$, one can calculate that $\lim_{k'_m \rightarrow \infty} \eta = i$. The same limit can be found for the case of unbounded mode losses $\lim_{k''_m \rightarrow \infty} \eta = i$. In both cases, therefore, the polarization tends to $S_1/S_0 = S_2/S_0 \rightarrow 0$ and $S_3/S_0 \rightarrow 1$, corresponding to the upper pole of the Poincaré sphere as depicted in Fig. 2 from the main text.

APPENDIX B: ANGULAR SPECTRUM OF AN ELECTRIC DIPOLE

The angular spectrum of a dipole source in a homogeneous medium has been derived previously in the literature [12,32,33,38,39], but here we present a very concise derivation. Our starting point is the vector potential of a dipole [32,40] given as $\mathbf{A} = -i\omega\mu\mathbf{p}\frac{e^{ikr}}{4\pi r}$ where ω is the angular frequency, μ is the magnetic permeability, $k = n\omega/c$ is the wave number and $r = |\mathbf{r} - \mathbf{r}_0|$ is the radial distance to the dipole position \mathbf{r}_0 , which we take as $\mathbf{r}_0 = \mathbf{0}$ below. The electromagnetic fields can be calculated from the potential as $\mathbf{H} = \frac{1}{\mu}\nabla \times \mathbf{A}$ and $\mathbf{E} = -\frac{1}{i\omega\epsilon}\nabla \times \mathbf{H}$. Combining these well-known definitions we can write the electric field of a dipole as

$$\mathbf{E}(\mathbf{r}) = \nabla \times \nabla \times \left(\frac{1}{\epsilon} \mathbf{p} \frac{e^{ikr}}{4\pi r} \right). \quad (\text{B1})$$

In order to find the angular spectrum, we need to perform a double spatial Fourier integral. To do this, we can use the well-known Weyl identity [38],

$$\frac{e^{i\mathbf{k}\cdot\mathbf{r}}}{r} = \frac{i}{2\pi} \iint_{-\infty}^{\infty} \frac{e^{i\mathbf{k}\cdot\mathbf{r}}}{k_z^{(+)}} dk_x dk_y, \quad (\text{B2})$$

where $\mathbf{r} = (x, y, z)$, $\mathbf{k} = (k_x, k_y, k_z)$ with the sign of $k_z = \pm\sqrt{k^2 - k_t^2}$ chosen depending on whether we are taking $z > 0$ or $z < 0$ such that $\text{Im}(k_z) > 0$ or $\text{Im}(k_z) < 0$, respectively, and where $k_z^{(+)}$ specifies having to take the sign for $z > 0$. Substituting Eq. (B2) into (B1), we can evaluate the curl ($\nabla \times$) operators inside the integral, which due to the harmonic dependence become ($i\mathbf{k} \times$) operators, resulting in

$$\mathbf{E}(\mathbf{r}) = \iint_{-\infty}^{\infty} \frac{1}{\varepsilon} \frac{i}{8\pi^2 k_z^{(+)}} [i\mathbf{k} \times i\mathbf{k} \times \mathbf{p}] e^{i\mathbf{k}\cdot\mathbf{r}} dk_x dk_y. \quad (\text{B3})$$

By simple comparison between Eq. (B3) and the definition of the angular spectrum in Eq. (5) of the main text, we immediately identify the angular spectrum of the dipole as the terms multiplying the exponential. This finalizes our derivation of the angular spectrum of the dipole. However, one may note that the angular spectrum is a vector quantity $\mathbf{E}(k_x, k_y)$, hence, in practice, it is useful to decompose it into its components in some basis.

A useful basis is the spherical basis, aligned with the relative orientation of the wave vector, defined by the unit vectors $\{\hat{\mathbf{e}}_k, \hat{\mathbf{e}}_p, \hat{\mathbf{e}}_s\}$ where we define $\hat{\mathbf{e}}_k = \mathbf{k}/k$, $\hat{\mathbf{e}}_s = (\hat{\mathbf{z}} \times \mathbf{k})/\sqrt{(\hat{\mathbf{z}} \times \mathbf{k}) \cdot (\hat{\mathbf{z}} \times \mathbf{k})}$, and $\hat{\mathbf{e}}_p = \hat{\mathbf{e}}_s \times \hat{\mathbf{e}}_k$ such that one can check they form an orthonormal basis $\hat{\mathbf{e}}_i \cdot \hat{\mathbf{e}}_j = \delta_{ij}$ with the interesting feature that the basis vectors are, in general, complex valued and yet our definition of orthonormality does not involve complex conjugation. This is possible thanks to the wave-equation Eq. (1) in the main text, which results in $\hat{\mathbf{e}}_k \cdot \hat{\mathbf{e}}_k = 1$. Thanks to this orthonormality, any vector can be expressed in terms of its components $\mathbf{p} = (\mathbf{p} \cdot \hat{\mathbf{e}}_k)\hat{\mathbf{e}}_k + (\mathbf{p} \cdot \hat{\mathbf{e}}_s)\hat{\mathbf{e}}_s + (\mathbf{p} \cdot \hat{\mathbf{e}}_p)\hat{\mathbf{e}}_p$. Therefore, making use of the fact that $\hat{\mathbf{e}}_k \times \hat{\mathbf{e}}_s = -\hat{\mathbf{e}}_p$ and $\hat{\mathbf{e}}_k \times \hat{\mathbf{e}}_p = \hat{\mathbf{e}}_s$ or using Lagrange's formula for the triple product, it is straightforward to show that $i\mathbf{k} \times i\mathbf{k} \times \mathbf{p} = -k^2(\hat{\mathbf{e}}_k \times \hat{\mathbf{e}}_k \times \mathbf{p}) = k^2[(\mathbf{p} \cdot \hat{\mathbf{e}}_s)\hat{\mathbf{e}}_s + (\mathbf{p} \cdot \hat{\mathbf{e}}_p)\hat{\mathbf{e}}_p]$ is simply a projection of \mathbf{p} into the space orthogonal to $\hat{\mathbf{e}}_k$. Substituting this into Eq. (B3), we arrive directly at

$$\mathbf{E}(\mathbf{r}) = \iint_{-\infty}^{\infty} \frac{ik^2}{8\pi^2 \varepsilon k_z^{(+)}} \mathbf{p} [(\hat{\mathbf{e}}_p)\hat{\mathbf{e}}_p + (\hat{\mathbf{e}}_s)\hat{\mathbf{e}}_s] e^{i\mathbf{k}\cdot\mathbf{r}} dk_x dk_y, \quad (\text{B4})$$

which completes the derivation of Eq. (6) in the main text.

-
- [1] M. Milosevic, *Appl. Spectrosc.* **67**, 126 (2013).
 [2] L. Marrucci, *Nat. Phys.* **11**, 9 (2015).
 [3] A. Aiello and P. Banzer, *J. Opt.* **18**, 085605 (2016).
 [4] K. Y. Bliokh, F. J. Rodríguez-Fortuño, F. Nori, and A. V. Zayats, *Nat. Photonics* **9**, 796 (2015).
 [5] A. Aiello, P. Banzer, M. Neugebauer, and G. Leuchs, *Nat. Photonics* **9**, 789 (2015).
 [6] K. Y. Bliokh, D. Smirnova, and F. Nori, *Science* **348**, 1448 (2015).
 [7] T. Van Mechelen and Z. Jacob, *Optica* **3**, 118 (2015).
 [8] F. J. Rodríguez-Fortuño, G. Marino, P. Ginzburg, D. O'Connor, A. Martínez, G. A. Wurtz, and A. V. Zayats, *Science* **340**, 328 (2013).
 [9] C. Junge, D. O'Shea, J. Volz, and A. Rauschenbeutel, *Phys. Rev. Lett.* **110**, 213604 (2013).
 [10] J. Petersen, J. Volz, and A. Rauschenbeutel, *Science* **346**, 67 (2014).
 [11] A. Espinosa-Soria and A. Martínez, *IEEE Photonics Technol. Lett.* **28**, 1561 (2016).
 [12] M. F. Picardi, A. Manjavacas, A. V. Zayats, and F. J. Rodríguez-Fortuño, *Phys. Rev. B* **95**, 245416 (2017).
 [13] F. J. Rodríguez-Fortuño, N. Engheta, A. Martínez, and A. V. Zayats, *Nat. Commun.* **6**, 8799 (2015).
 [14] F. Kalthor, T. Thundat, and Z. Jacob, *Appl. Phys. Lett.* **108**, 061102 (2016).
 [15] J. J. Kingsley-Smith, M. F. Picardi, L. Wei, A. V. Zayats, and F. J. Rodríguez-Fortuño, *Phys. Rev. B* **99**, 235410 (2019).
 [16] S. Sukhov, V. Kajorndejnkul, R. R. Naraghi, and A. Dogariu, *Nat. Photonics* **9**, 809 (2015).
 [17] C. Sayrin, C. Junge, R. Mitsch, B. Albrecht, D. O'Shea, P. Schneeweiss, J. Volz, and A. Rauschenbeutel, *Phys. Rev. X* **5**, 041036 (2015).
 [18] J. Ma, X. Xi, Z. Yu, and X. Sun, *Appl. Phys. Lett.* **108**, 151103 (2016).
 [19] F. J. Rodríguez-Fortuño, I. Barber-Sanz, D. Puerto, A. Griol, and A. Martínez, *ACS Photonics* **1**, 762 (2014).
 [20] Z. Shao, J. Zhu, Y. Chen, Y. Zhang, and S. Yu, *Nat. Commun.* **9**, 926 (2018).
 [21] L. Wei and F. J. Rodríguez-Fortuño, *New J. Phys.* **22**, 083016 (2020).
 [22] Y. Long, H. Ge, D. Zhang, X. Xu, J. Ren, M.-H. Lu, M. Bao, H. Chen, and Y.-F. Chen, *Natl. Sci. Rev.* **7**, 1024 (2020).
 [23] S. Golat, E. A. Lim, and F. J. Rodríguez-Fortuño, *Phys. Rev. D* **101**, 084046 (2020).
 [24] A. B. Young, A. C. T. Thijssen, D. M. Beggs, P. Androvitsaneas, L. Kuipers, J. G. Rarity, S. Hughesand, and R. Oulton, *Phys. Rev. Lett.* **115**, 153901 (2015).
 [25] B. Feber, N. Rotenberg, and L. Kuipers, *Nat. Commun.* **6**, 6695 (2015).
 [26] J. E. Vázquez-Lozano, A. Martínez, and F. J. Rodríguez-Fortuño, *Phys. Rev. Appl.* **12**, 024065 (2019).
 [27] A. K. Benjamin Krüger and T. Brenner, *Opt. Express* **25**, 25165 (2017).
 [28] C. A. Balanis, *Advanced Engineering Electromagnetics* (John Wiley & Sons, New York, 1989).
 [29] D. O'Connor, P. Ginzburg, F. J. Rodríguez-Fortuño, G. A. Wurtz, and A. V. Zayats, *Nat. Commun.* **5**, 5327 (2014).
 [30] M. F. Picardi, M. Neugebauer, J. S. Eismann, G. Leuchs, P. Banzer, F. J. Rodríguez-Fortuño, and A. V. Zayats, *Light: Sci. Appl.* **8**, 52 (2019).
 [31] M. F. Picardi, A. V. Zayats, and F. J. Rodríguez-Fortuño, *Laser Photon. Rev.* **13**, 1900250 (2019).

- [32] L. Novotny and B. Hecht, *Principles of Nano-Optics*, 1st ed. (Cambridge University Press, New York, 2006).
- [33] N. Rotenberg, M. Spasenović, T. L. Krijger, B. le Feber, F. J. García de Abajo, and L. Kuipers, *Phys. Rev. Lett.* **108**, 127402 (2012).
- [34] N. Kinsey, C. DeVault, A. Boltasseva, and V. Shalaev, *Nat. Rev. Mater.* **4**, 742 (2019).
- [35] F. Perrin, *J. Chem. Phys.* **10**, 415 (1942).
- [36] E. Collett, *Field Guide to Polarization* (SPIE, Bellingham, WA, 2005).
- [37] K. Y. Bliokh and F. Nori, *Phys. Rep.* **592**, 1 (2015).
- [38] L. Mandel and E. Wolf, *Optical Coherence and Quantum Optics*, 1st ed. (Cambridge University Press, New York, 1995).
- [39] M. F. Picardi, Ph.D. thesis, King's College London, 2020.
- [40] A. Ishimaru, *Electromagnetic Wave Propagation, Radiation and Scattering* (Wiley-IEEE Press, Piscataway, NJ, 2017).